www.czasopisma.pan.pl PAN POLSKA AKADEMIA NAUK www.journals.pan.pl

BULLETIN OF THE POLISH ACADEMY OF SCIENCES
TECHNICAL SCIENCES, Vol. 73(4), 2025, Article number: e154281
DOI: 10.24425/bpasts.2025.154281

SPECIAL SECTION

Sensorless control with multi-scalar transformation of five-phase IPMSM

Deepak VYAS [1,2] *, Shahal Ibn Islam JOY [1], Marcin MORAWIEC [1], Grzegorz KOSTRO [1], Łukasz SIENKIEWICZ [1], and Nirav JOSHI [3]

[1] Faculty of Electrical and Control Engineering, Gdańsk University of Technology, ul. Narutowicza 11/12, 80-233 Gdańsk, Poland
[2] Department of Electrical Engineering, School of Energy Technology, Pandit Deendayal Energy University, Raisan, Gandhinagar-382426, Gujarat, India
[3] Department of Electrical Engineering, Marwadi University, Rajkot, Gujarat, India

Abstract. This article proposes sensorless multiscalar control for a multiphase interior permanent magnet synchronous machine. The chosen parameters are estimated using an adaptive observer structure. In the proposed solution, the machine model vector form is in the stationary reference frame $(\alpha\beta)$, and transformation to (dq) – the coordinate system is unnecessary to implement the proposed control structure. In the control structure, the nonlinear model linearization is based on demonstrated nonlinear variables transformation for $(\alpha\beta)_{(i)}$ orthogonal planes. Using the proposed control technique, mechanical and electromagnetic subsystems are decoupled, which is the main advantage of this control structure. To provide a comparative analysis, the proposed multiscalar control structure is also compared with the existing multiscalar control scheme. Finally, the simulation and experimental results are demonstrated to validate the performance of the proposed control solution for a sensorless five-phase interior permanent magnet synchronous motor test setup.

Keywords: multi-phase machine; nonlinear control; sensorless control.

NOMENCLATURE

ψ_f	Permanent magnet flux
T_e	Electro-magnetic torque
T_L	Load torque
J	Moment of inertia
ω_r	Rotor speed
θ_r	Rotor angle
$x_{11}, x_{12}, x_{21}, x_{22}$	Multiscalar variables
(i)	Index of control system (1st or 2nd plane)
$\hat{x}$	Estimated variable
$\tilde{x}$	Estimation error
x^*	Reference value
$u_{s\alpha}, u_{s\beta}$	Components of stator voltage in stationary coordinates system
$i_{s\alpha}, i_{s\beta}$	Components of stator current in stationary coordinates system
$\psi_{s\alpha}, \psi_{s\beta}$	Components of stator flux in stationary coordinates system
$\psi_{f\alpha}, \psi_{f\beta}$	Components of permanent magnet flux in stationary coordinates system
ψ_f^α	Active flux linkage

*e-mail: deevyas@pg.edu.pl

Manuscript submitted 2024-09-13, revised 2025-03-13, initially accepted for publication 2025-04-02, published in July 2025.

1. INTRODUCTION

Multiphase machines are widely acknowledged due to their special advantages: increment in torque density, enhancement in reliability and power density, higher fault tolerance capability, reduction in DC link stress, and lower torque ripple. Multiphase machines can be used in various applications such as electromobility (electric vehicle), electric aircraft, ship propulsion, and electric traction drives. A five-phase permanent magnet synchronous motor is one the most suitable representative of a multiphase motor because of its higher torque density, fast dynamic response, higher reliability, and good power factor [1–4]. In a multiphase machine, it is possible to enhance the torque component by injecting harmonic current into the phase currents [5]. Moreover, components of each current harmonics can be represented separately in the space vector plane. Generally, less than the total number of phases are selected for injection harmonic order.

In order to remove the demerits of position sensors [6], sensorless control techniques are preferred. Sensorless control techniques are categorized in two ways. In the first approach, saliency-based methods are preferred specifically for zero and low-speed operation ranges, while in the second approach, model-based methods are popular for medium-speed and high-speed operation ranges [6–9].

Research on the multiphase machine is majorly focused on the improvement of fault-tolerant capability [10–13]. Various control strategies for three-phase machine applications have been extended to control multiphase machines. The field-oriented control (FOC) in which state variables are oriented in a rotating reference frame (dq) and direct torque control (DTC) are the most commonly used control strategies for multiphase machines. These approaches are well explained in the literature by researchers across the world [14–17].

The main drawback of the vector control scheme is that while changing the flux linkage, the decoupling between the electromagnetic and electro-mechanical parts is not achieved in the presence of nonlinearities defined in [3]. It fails to decouple the system completely in the presence of nonlinearity due to the machine state variable transformation to the rotating reference frame (dq), and plausible intervention between the two controlled subsystems of the multiphase machine. Hence, three-phase machine transformation into the linear form was generalized for multi-input, multi-output systems [18].

To obtain the enhanced transient response and minimize the tracking error, a generalized deadbeat solution for model predictive control of five-phase IPMSM was proposed [19]. To control the six-phase PMSM, a Luenberger observer with MPC was employed [20]. Luenberger observer with MPC focused on compensating localization error of the reference vector due to machine parameter mismatch. This control approach enhanced the steady state performance of drive and robustness. Disturbance observer-based predictive control of six-phase IPMSM was reported in [21] to reduce the harmonic components. This control system provided reliable and adequate performance for different values of dead time in the power converter. In [22], a novel fractional integral terminal sliding mode controller (FITSMC) is proposed for five-phase IPMSM. This control system facilitates additional convergence which minimizes the tracking errors and also minimizes oscillations in the case of open-phase faults. FITSMC provided enhanced performance than the classical sliding mode control and proportional-integral (PI) controllers. High frequency (HF) square wave injection into the second plane-based sensorless control of a five-phase IPMSM drive is presented [23]. The control strategy allowed us to reduce the torque ripple and improved the overall control structure of the five-phase drive system.

There is no discussion on control using nonlinear feedback for five-phase IPMSM in the existing literature. This article proposes a control system that applies x-nonlinear variables-based sensorless control for a five-phase interior permanent magnet synchronous machine (IPMSM). In the proposed control technique, nonlinear feedback is utilized to linearize the selected x-nonlinear variables and then obtain final control signals to generate the gate pulse for the five-phase inverter to operate the five-phase IPMSM drives. Compared with FOC, the proposed control technique reduces mathematical computation by eliminating the need for the reference frame transformation to the (dq) coordinate system. The proposed control scheme establishes accurate decoupling of electromagnetic and mechanical sub-systems, while FOC-based control structures have limitations in decoupling the nonlinear machine model.

In the case of five-phase IPMSM, the third current harmonic will be injected to improve the utilization of electromagnetic torque. An adaptive speed observer is used to reconstruct the state variables: stator currents components, angular speed, and angular position. Analytical, simulation and experimental tests examine and validate this proposed control structure. The experimental tests were conducted on 5.5 kW five-phase IPMSM in sensorless operation with the third harmonic injection.

The main contributions of the article are:

1. Proposition of multiscalar control scheme of five-phase IPMSM.
2. Comparative analysis with classical multiscalar control structure.
3. Elimination of a PI controller in each plane for electromagnetic subsystems.
4. Simulation and experimental confirmation of the developed control solution under selected working points of the five-phase IPMSM

The paper is structured in the following manner. Section 2 and Section 3 cover the mathematical model and observer structure of the five-phase IPMSM drive, respectively. Section 4 and Section 5 explain the classical multiscalar control system and proposed multiscalar control system, respectively. In Section 6, simulation and experimental results are discussed in detail, followed by a conclusion in Section 7.

2. MATHEMATICAL MODEL OF FIVE-PHASE IPMSM

The mathematical model of a five-phase machine can be developed similarly to three-phase machines [24–27]. In this article, the mathematical model of the five-phase IPMSM is expressed in the per-unit system except for time. However, certain adaption is required. For example, for the five-phase IPMSM, phase displacement is 72° between each phase. Due to the injection of the current harmonic, the machine model can be transformed from a natural reference frame (a-b-c-d-e) to two stationary orthogonal planes for fundamental components and the third harmonic components, respectively. Machine analysis is done sincerely in a stationary reference frame in this article. The mathematical model of IPMSM is well-known in the literature. The mathematical form of the five-phase IPMSM in the vector form using differential equations can be prepared as

$$\frac{\mathrm{d}i_{s\alpha(i)}}{\mathrm{d}t} = -\frac{1}{L_{q(i)}}R_s i_{s\alpha(i)} + \frac{1}{L_{q(i)}}\omega_{r(i)}\psi_{f\beta(i)} + \frac{1}{L_{q(i)}}u_{s\alpha(i)}, \tag{1}$$

$$\frac{\mathrm{d}i_{s\beta(i)}}{\mathrm{d}t} = -\frac{1}{L_{q(i)}}R_s i_{s\beta(i)} - \frac{1}{L_{q(i)}}\omega_{r(i)}\psi_{f\alpha(i)} + \frac{1}{L_{q(i)}}u_{s\beta(i)}, \tag{2}$$

$$\frac{\mathrm{d}\omega_{r(i)}}{\mathrm{d}t} = \frac{1}{J}\left(\sum_{i=1}^{N}\left(\psi_{f\alpha(i)}i_{s\beta(i)} - \psi_{f\beta(i)}i_{s\alpha(i)}\right) - T_L\right), \tag{3}$$

$$\frac{\mathrm{d}\theta_{r(i)}}{\mathrm{d}t} = \omega_{r(i)}. \tag{4}$$

It is important to note that index i defines the reference plane for multiphase IPMSM. Where $i = 1$ for fundamental plane and $i = 2$ for the second plane, R_s is stator resistance, $L_{q(i)}$ is q-axis inductance, $\omega_{r(i)}$ is rotor speed, T_L is load torque, J is the rotor moment of inertia, $u_{s\alpha(i)}$ and $u_{s\beta(i)}$ are stator voltage components, $i_{s\alpha(i)}$ and $i_{s\beta(i)}$ are the stator current components, $\psi_{f\alpha(i)}$ and $\psi_{f\beta(i)}$ are the permanent magnet flux components for the first plane and second plane, respectively. It is assumed that machine parameters for five-phase IPMSM are known and constant. A brief description of observer structure is given in the next section.

3. OBSERVER STRUCTURE OF FIVE-PHASE IPMSM

From the mathematical model of the five-phase IPMSM defined in (1) to (4), speed and position observer structure can be prepared for the first and second planes in stationary reference frames. "ˆ" denotes the estimated state variable, and "˜" denotes the error between the estimated and measured quantity.

$$\frac{\mathrm{d}\hat{i}_{s\alpha(i)}}{\mathrm{d}t} = -\frac{1}{L_{q(i)}}R_s\hat{i}_{s\alpha(i)} + \frac{1}{L_{q(i)}}\hat{\omega}_{(i)}\hat{\psi}_{f\beta(i)} + \frac{1}{L_{q(i)}}u_{s\alpha(i)} + v_{\alpha(i)}, \tag{5}$$

$$\frac{\mathrm{d}\hat{i}_{s\beta(i)}}{\mathrm{d}t} = -\frac{1}{L_{q(i)}}R_s\hat{i}_{s\beta(i)} - \frac{1}{L_{q(i)}}\hat{\omega}_{(i)}\hat{\psi}_{f\alpha(i)} + \frac{1}{L_{q(i)}}u_{s\beta(i)} + v_{\beta(i)}, \tag{6}$$

$$\frac{\mathrm{d}\hat{\theta}_{(i)}}{\mathrm{d}t} = \hat{\omega}_{(i)}, \tag{7}$$

$$\begin{aligned}\hat{\psi}_{f\alpha(i)} &= \psi_f\cos\hat{\theta}_{r(i)},\\ \hat{\psi}_{s\alpha(i)} &= L_q\hat{i}_{s\alpha(i)} + \hat{\psi}_{f\alpha(i)},\end{aligned} \tag{8}$$

$$\begin{aligned}\hat{\psi}_{f\beta(i)} &= \psi_{f(i)}\sin\hat{\theta}_{r(i)},\\ \hat{\psi}_{s\beta(i)} &= L_q\hat{i}_{s\beta(i)} + \hat{\psi}_{f\beta(i)},\end{aligned} \tag{9}$$

$$\begin{aligned}\tilde{i}_{s\alpha,\beta(i)} &= \hat{i}_{s\alpha,\beta(i)} - i_{s\alpha,\beta(i)},\\ \tilde{\omega}_{r(i)} &= \hat{\omega}_{r(i)} - \omega_{r(i)},\\ \tilde{\theta}_{r(i)} &= \hat{\theta}_{r(i)} - \theta_{r(i)},\end{aligned} \tag{10}$$

where current components are $(\hat{i}_{s\alpha(i)})$ and $(\hat{i}_{s\beta(i)})$, and stator flux components are $(\hat{\psi}_{s\alpha(i)})$ and $(\hat{\psi}_{s\beta(i)})$, calculated using the estimated angular position in each plane. To achieve asymptotic stability, stabilizing functions $(v_{\alpha(i)})$ and $(v_{\beta(i)})$ are added in (5) and (6).

The Lyapunov stability criteria are employed to design the final form of the stabilizing functions [28]. The error between the estimated and measured state variables can be calculated using (10). To estimate the angular speed, classical adaptive control law was applied [28–30]. Rotor speed can be estimated using (11)

$$\dot{\hat{\omega}}_{r(i)} = -\gamma_{(i)}\left(\hat{\psi}_{f\beta(i)}\tilde{i}_{s\alpha(i)} - \hat{\psi}_{f\alpha(i)}\tilde{i}_{s\beta(i)}\right) \quad \text{for } \gamma > 0. \tag{11}$$

4. CLASSICAL MULTISCALAR CONTROL OF THE FIVE-PHASE IPMSM

It is important to mention that discussion on multiscalar control is only available for three-phase PMSM in the literature [3, 31]. To conduct a comparative analysis with the proposed control scheme, the classical control structure is extended for the five-phase IPMSM in this article. In the control scheme, a new model of the machine is prepared with state variables (x). The stator current vector $(\boldsymbol{i}_{s(i)})$ and stator flux vector $(\boldsymbol{\psi}_{s(i)})$ can be transformed into the scalar variables by the inner and external product operation. The new state variables considering $(\boldsymbol{i}_{s(i)}, \boldsymbol{\psi}_{s(i)})$ for the five-phase IPMSM are angular rotor speed $(x_{11(i)})$, vector product of stator current vector, and stator flux vector $(x_{12(i)})$, which is proportional to the motor torque component, the square of the stator flux $(x_{21(i)})$ and scalar product of stator current and stator flux vector $(x_{22(i)})$ which is flux controlling variable, respectively. The chosen state variables are represented as

$$x_{11(i)} = \omega_{r(i)}, \tag{12}$$

$$x_{12(i)} = \psi_{s\alpha(i)}i_{s\beta(i)} - \psi_{s\beta(i)}i_{s\alpha(i)}, \tag{13}$$

$$x_{21(i)} = \psi^2_{s\alpha(i)} + \psi^2_{s\beta(i)}, \tag{14}$$

$$x_{22(i)} = \psi_{s\alpha(i)}i_{s\alpha(i)} + \psi_{s\beta(i)}i_{s\beta(i)}. \tag{15}$$

The new nonlinear mathematical model for the five-phase IPMSM drive is presented here by taking the time derivative of nonlinear variables from (12) to (15) variables and substituting the derivative of currents and stator fluxes; the final form is given as

$$\frac{\mathrm{d}x_{11(i)}}{\mathrm{d}t} = \frac{1}{J}x_{12(i)} - \frac{1}{J}T_L, \tag{16}$$

$$\frac{\mathrm{d}x_{12(i)}}{\mathrm{d}t} = -\frac{1}{T_{v(i)}}x_{12(i)} - \frac{1}{L_{q(i)}}x_{11(i)}\left(\psi_{s(i)}\odot\psi_{f(i)}\right) + q_{s(i)} + u_{1(i)}, \tag{17}$$

$$\frac{\mathrm{d}x_{21(i)}}{\mathrm{d}t} = 2\left(-R_s x_{22(i)} + u_{s\alpha(i)}\psi_{s\alpha(i)} + u_{s\beta(i)}\psi_{s\beta(i)}\right), \tag{18}$$

$$\frac{\mathrm{d}x_{22(i)}}{\mathrm{d}t} = -\frac{1}{T_{v(i)}}x_{22(i)} - R_s i^2_{s(i)} + \frac{1}{L_{q(i)}}x_{11(i)}\left(\psi_{s(i)}\otimes\psi_{f(i)}\right) + p_{s(i)} + u_{2(i)}, \tag{19}$$

where $(T_{v(i)})$ is the motor electromagnetic time constant and other various terms that appear in differential equations from (16) to (19) are given as

$$T_{v(i)} = \frac{L_{q(i)}}{R_s}, \tag{20}$$

$$\left(\psi_{s(i)}\odot\psi_{f(i)}\right) = \left(\psi_{s\alpha(i)}\psi_{f\alpha(i)} + \psi_{s\beta(i)}\psi_{f\beta(i)}\right), \tag{21}$$

$$\left(\psi_{s(i)}\otimes\psi_{f(i)}\right) = \left(\psi_{s\alpha(i)}\psi_{f\beta(i)} - \psi_{s\beta(i)}\psi_{f\alpha(i)}\right), \tag{22}$$

$$p_{s(i)} = u_{s\alpha(i)}i_{s\alpha(i)} + u_{s\beta(i)}i_{s\beta(i)}, \tag{23}$$

$$q_{s(i)} = u_{s\alpha(i)}i_{s\beta(i)} - i_{s\alpha(i)}u_{s\beta(i)}, \tag{24}$$

$$i^2_{s(i)} = \left(i^2_{s\alpha(i)} + i^2_{s\beta(i)}\right), \tag{25}$$

$$u_{1(i)} = \frac{1}{L_{q(i)}}\left(\psi_{s\alpha(i)}u_{s\beta(i)} - \psi_{s\beta(i)}u_{s\alpha(i)}\right), \tag{26}$$

$$u_{2(i)} = \frac{1}{L_{q(i)}}\left(\psi_{s\alpha(i)}u_{s\alpha(i)} + \psi_{s\beta(i)}u_{s\beta(i)}\right). \tag{27}$$

In the next step, the feedback linearization process must be completed. To linearize the nonlinear system, new signals

$(m_{1(i)})$ and $(m_{2(i)})$ are computed using PI controllers of $(x_{12(i)})$ and $(x_{22(i)})$ as shown in Fig. 1.

$$m_{1(i)} = -\frac{1}{L_{q(i)}} x_{11(i)} (\psi_{s(i)} \odot \psi_{f(i)}) + q_{s(i)} + u_{1(i)}, \tag{28}$$

$$m_{2(i)} = -R_s i_{s(i)}^2 + \frac{1}{L_{q(i)}} x_{11(i)} (\psi_{s(i)} \otimes \psi_{f(i)}) + p_{s(i)} + u_{2(i)}, \tag{29}$$

where $(u_{1(i)})$ and $(u_{2(i)})$ are the control signals appearing in the nonlinear model of IPMSM. The pulse width modulation (PWM) algorithm needs voltage components that can be calculated from the defined control signals.

$$u_{s\alpha(i)} = L_{q(i)} \left(\frac{u_{2(i)} \psi_{s\alpha(i)} - u_{1(i)} \psi_{s\beta(i)}}{x_{21(i)}} \right), \tag{30}$$

$$u_{s\beta(i)} = L_{q(i)} \left(\frac{u_{2(i)} \psi_{s\beta(i)} + u_{1(i)} \psi_{s\alpha(i)}}{x_{21(i)}} \right). \tag{31}$$

A control system structure based on stator current and flux is depicted in Fig. 1. Two linear subsystems are controlled by cascaded controllers. An electromechanical subsystem is presented in (32) and (33) whereas an electromagnetic subsystem is shown in (34) and (35).

$$\frac{\mathrm{d}x_{11(i)}}{\mathrm{d}t} = \frac{1}{J} x_{12(i)} - \frac{1}{J} T_L, \tag{32}$$

$$\frac{\mathrm{d}x_{12(i)}}{\mathrm{d}t} = -\frac{1}{T_{v(i)}} x_{12(i)} + m_{1(i)}, \tag{33}$$

$$\frac{\mathrm{d}x_{21(i)}}{\mathrm{d}t} = 2(-R_s x_{22(i)} + u_{s\alpha(i)} \psi_{s\alpha(i)} + u_{s\beta(i)} \psi_{s\beta(i)}), \tag{34}$$

$$\frac{\mathrm{d}x_{22(i)}}{\mathrm{d}t} = -\frac{1}{T_{v(i)}} x_{22(i)} + m_{2(i)}. \tag{35}$$

Controllers marked in red line are for the first plane and in green line are for the second plane of the five-phase IPMSM. From Fig. 1, it can be observed that seven controllers are required to implement the classical control scheme.

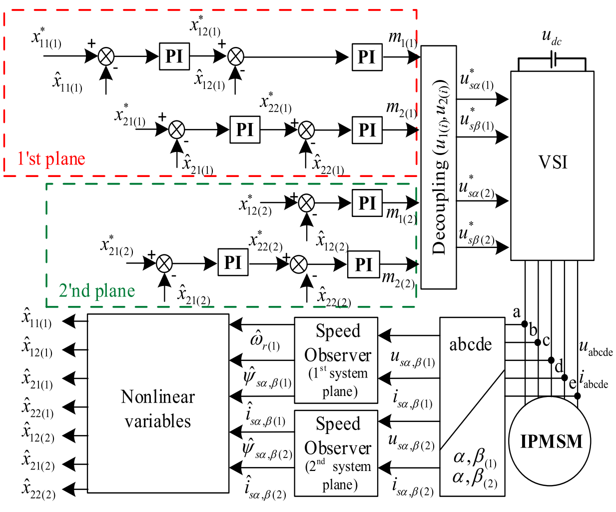

Fig. 1. Classical multiscalar control for five-phase IPMSM

5. PROPOSED MULTISCALAR CONTROL FOR FIVE-PHASE IPMSM

The presented control structure in Section 4 is depicted in Fig. 1, where four PI controllers in the first plane and three controllers in the second plane are mandatory for control of five-phase IPMSM. Based on the dependences for the multiscalar model (16)–(19), control variables occur in (17) and (19). From control variables $(u_{1(i)})$ and $(u_{2(i)})$, voltage components $(u_{s\alpha(i)})$ and $(u_{s\beta(i)})$ are calculated in stationary reference frame as was discussed in Section 4. In comparison with the classical control structure, stationary voltage components can be obtained from control signals appearing in (17) and (18) in the proposed control structure. In the proposed solution, without referring (19), both control signals can be obtained which eliminates one PI controller in each plane in the electromagnetic subsystem. The new control signal $m_{1(i)}$ can be computed from the $(x_{12(i)})$ controller as discussed earlier. Using the proposed approach, $m_{2(i)}$ can be calculated from the $(x_{21(i)})$ controller only in each plane. It is important to mention that the form of the control signal $(u_{1(i)})$ remains the same as (26), while the control signal $(u_{2(i)})$ is shown in (36). Using the proposed control structure of the five-phase IPMSM, it is possible to control flux controlling variable $(x_{22(i)})$ internally from the $(x_{21(i)})$ controller only

$$u_{2(i)} = 2(\psi_{s\alpha(i)} u_{s\alpha(i)} + \psi_{s\beta(i)} u_{s\beta(i)}). \tag{36}$$

The block diagram of the proposed control system is shown in Fig. 2. To implement the proposed control structure a total of five controllers are required.

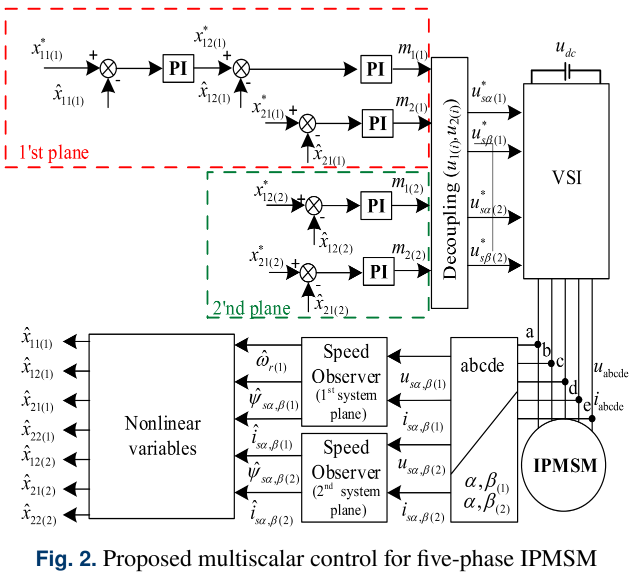

Fig. 2. Proposed multiscalar control for five-phase IPMSM

From the PI controllers of $(x_{12(i)})$ and $(x_{21(i)})$, feedback signals $(m_{1(i)})$ and $(m_{2(i)})$ are calculated for linearization process as shown in Fig. 2. $(u_{1(i)})$ and $(u_{2(i)})$ are the control variables appearing in the nonlinear model of IPMSM (17), (19) and after transforming to voltage components as (37), (38).

$$u_{s\alpha(i)} = -\frac{1}{2x_{21(i)}} (2L_{q(i)} u_{1(i)} \psi_{s\beta(i)} - u_{2(i)} \psi_{s\alpha(i)}), \tag{37}$$

$$u_{s\beta(i)} = \frac{1}{2x_{21(i)}}\left(2L_{q(i)}u_{1(i)}\psi_{s\alpha(i)} + u_{2(i)}\psi_{s\beta(i)}\right). \tag{38}$$

After completing the process of linearization and decoupling, two linear and fully decoupled subsystems are obtained: the electromechanical subsystem remains the same as (32) and (33) while the electromagnetic subsystem changes to (39)

$$\frac{\mathrm{d}x_{21(i)}}{\mathrm{d}t} = -2R_s x_{22(i)} + u_{2(i)}\,. \tag{39}$$

6. RESULTS AND DISCUSSION

6.1. Simulation results

In Fig. 3 and Fig. 4 chosen simulation results using measured parameters are shown. The five-phase IPMSM drive starting up to 1.0 p.u. is shown using a multiscalar control scheme in Fig. 3a, and using the proposed control scheme in Fig. 3b. Nonlinear variables such as the speed of the first plane ($x_{11(1)}$), the torque produced in the first plane ($x_{12(1)}$) and the second plane ($x_{12(2)}$) during the transient state, the square of stator flux ($x_{21(1)}$), and flux controlling variable ($x_{22(1)}$) are depicted. It can be observed that mechanical subsystems and electromagnetic subsystems are decupled and controlled separately. To maintain the flux level constant flux controlling variable ($x_{22(1)}$) is controlled internally by the square of the flux controller in the proposed control scheme, while in the classical control scheme, additional controllers are required to control the flux controlling variable ($x_{22(1)}$) and ($x_{22(2)}$) to achieve decoupling between mechanical and electromagnetic subsystems.

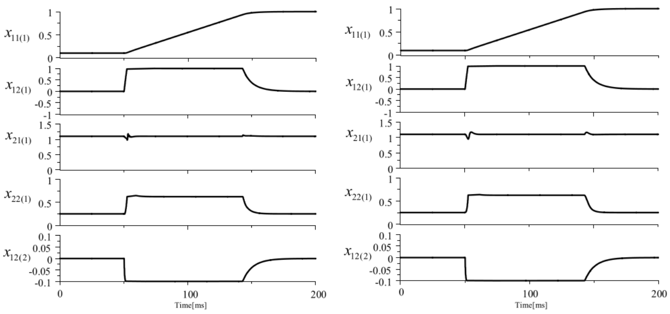

(a) (b)

Fig. 3. Simulation result of the five-phase IPMSM starting up to 1.0 p.u. (a) classical multiscalar control structure, (b) proposed multiscalar control structure

In Fig. 4, the drive reversing from 1.0 p.u. to −1.0 p.u. with applied load around 0.5 p.u. The performance of the classical multiscalar control system and the proposed control system for the multiphase IPMSM are shown in Fig. 4a and Fig. 4b, respectively. The angular speed of the first plane ($x_{11(1)}$) and the second plane ($x_{11(2)}$), the torque generated in the first plane ($x_{12(1)}$) and the second plane ($x_{12(2)}$) in the dynamic state and square of stator flux in the first plane ($x_{21(1)}$) are shown. The angular speed of the second plane ($x_{11(2)}$) reverses from −3.0 p.u. to 3.0 p.u., the torque is limited to 1.0 p.u. for the first plane

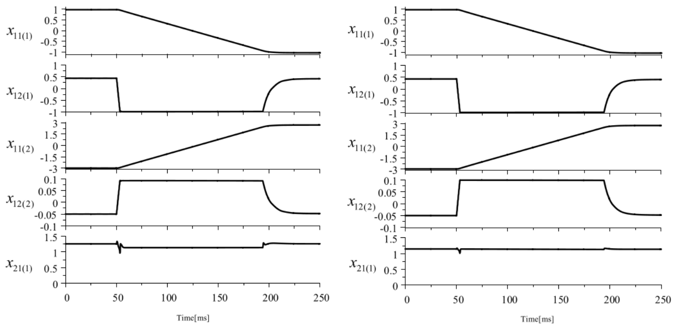

(a) (b)

Fig. 4. Simulation result of the five-phase IPMSM reversing from 1.0 p.u. to −1.0 p.u. (a) classical multiscalar control structure, (b) proposed multiscalar control structure

($x_{12(1)}$) and 0.1 p.u. for the second plane ($x_{12(2)}$) during the dynamic state. The flux level is kept constant at 1.1 p.u. in the first plane ($x_{21(1)}$), as shown in Fig. 4b. During the drive reversal, stator flux is maintained at 1.1 p.u. using the proposed control solution but classical control structure fails to remain at 1.1 p.u. during the dynamic state. The proposed multiscalar control ensures proper decoupling between the electromechanical and electromagnetic subsystems. From the simulation results, it can be observed that the proposed control structure for the five-phase IPMSM provides similar results to the classical control system with a smaller number of controllers. To confirm the theoretical hypothesis, the chosen experimental results are discussed.

6.2. Experimental results

The performance of the proposed control system in real-time operating conditions was evaluated precisely using the set of laboratory equipment. In the experimental set, a 5.5 kW five-phase IPMSM drive system fed by a voltage source converter (VSC) was used. The parameters of the five-phase IPMSM used for experimental tests are defined in Table 1. For control system implementation, DSP SHARC ADSP21363 floating-point signal processor and Altera Cyclone 2 FPGA were used in the interface with a sampling time of 150 µs. The transistor switching frequency of the inverter was 3.3 kHz. Control system implementation in the DSP board is shown in Fig. 1 and Fig. 2. LA 25-NP transducer was used to measure the currents in the natural reference frame and then transformed to the stationary reference frame ($\alpha\beta$) using the Clarke transformation for observer structure execution. The incremental encoder (11 bits) was employed to measure the speed of the five-phase IPMSM. It is important to mention that the encoder was only used to substantiate the estimation accuracy of the observer structure. Tuning gains of the PI controllers for the classical control structure are given in Table 2, and for proposed control structure are given in Table 3.

The tracking responses of the "x" nonlinear variables in $(\alpha\beta)_{(i)}$ coordinates for a drive starting up to nominal speed using the classical control and the proposed control schemes are shown in Fig. 5. Estimated parameters are used for the control of

Table 1
IPMSM parameters and reference unit

Symbol	Quantity	Values
R_{sn}	Stator resistance	0.0680 p.u.
$L_{dn(1)}$	$d_{(1)}$-axis inductance	0.4263 p.u.
$L_{dn(2)}$	$d_{(2)}$-axis inductance	0.1421 p.u.
$L_{qn(1)}$	$q_{(1)}$-axis inductance	0.6484 p.u.
$L_{qn(2)}$	$q_{(2)}$-axis inductance	0.2161 p.u.
P	Pole pairs	3
P_n	Nominal power	5.5 kW
T_{en}	Nominal value of torque	0.8817 p.u.
$\psi_{f(1)}$	Permanent magnets flux linkage $_{(1)}$	0.89 p.u.
$\psi_{f(2)}$	Permanent magnets flux linkage $_{(2)}$	0.07 p.u.
U_n	Nominal stator voltage (Y)	275 V
I_n	Nominal stator current (Y)	10.2 A
n	Nominal rotor speed	1500 rpm
f	Nominal frequency	75 Hz
$U_b = U\mathrm{n}$	Reference voltage	275 V
$I_b = In\sqrt{5}$	Reference current	22.80 A

Table 2
Tuning gains of the multiscalar control structure

Symbol	Quantity	Values
$k_{px11(1)}$	Proportional gain for $x_{11(1)}$ controller	7.5
$k_{ix11(1)}$	Integral gain for $x_{11(1)}$ controller	0.001
$k_{px12(1)}$	Proportional gain for $x_{12(1)}$ controller	7.5
$k_{ix12(1)}$	Integral gain for $x_{12(1)}$ controller	0.1
$k_{px21(1)}$	Proportional gain for $x_{21(1)}$ controller	5
$k_{ix21(1)}$	Integral gain for $x_{21(1)}$ controller	0.1
$k_{px22(1)}$	Proportional gain for $x_{22(1)}$ controller	1.8
$k_{ix22(1)}$	Integral gain for $x_{22(1)}$ controller	0.1
$k_{px12(2)}$	Proportional gain for $x_{12(2)}$ controller	5
$k_{ix12(2)}$	Integral gain for $x_{12(2)}$ controller	0.1
$k_{px21(2)}$	Proportional gain for $x_{21(2)}$ controller	5
$k_{ix21(2)}$	Integral gain for $x_{21(2)}$ controller	0.1
$k_{px22(2)}$	Proportional gain for $x_{22(2)}$ controller	2
$k_{ix22(2)}$	Integral gain for $x_{22(2)}$ controller	0.1

the multiphase IPMSM. The reference command of stator flux was 1.1 p.u. for the first plane and 0.1 p.u. for the second plane $(x^*_{21(1)})$ and $(x^*_{21(2)})$, respectively.

In Fig. 5a and 5b, variables such as measured machine speed $(x_{11(1)})$, estimated speed $(\hat{x}_{11(1)})$, speed estimation error $(\tilde{x}_{11(1)})$, measured current component $(i_{s\alpha(1)})$, and estimated current component $(\hat{i}_{s\alpha(1)})$ are shown.

Table 3
Tuning gains of the proposed multiscalar control structure

Symbol	Quantity	Values
$k_{px11(1)}$	Proportional gain for $x_{11(1)}$ controller	7.5
$k_{ix11(1)}$	Integral gain for $x_{11(1)}$ controller	0.001
$k_{px12(1)}$	Proportional gain for $x_{12(1)}$ controller	7.5
$k_{ix12(1)}$	Integral gain for $x_{12(1)}$ controller	0.1
$k_{px21(1)}$	Proportional gain for $x_{21(1)}$ controller	7.5
$k_{ix21(1)}$	Integral gain for $x_{21(1)}$ controller	0.1
$k_{px12(2)}$	Proportional gain for $x_{12(2)}$ controller	5
$k_{ix12(2)}$	Integral gain for $x_{12(2)}$ controller	0.1
$k_{px21(2)}$	Proportional gain for $x_{21(2)}$ controller	5
$k_{ix21(2)}$	Integral gain for $x_{21(2)}$ controller	0.1

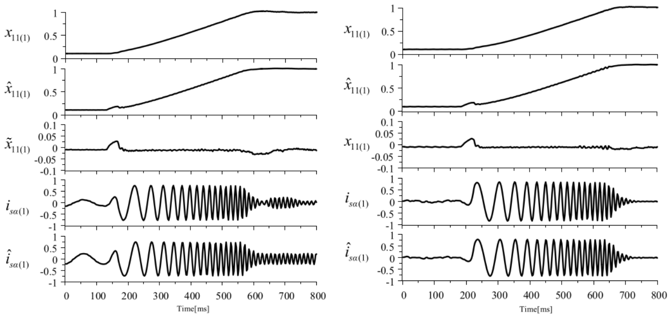

(a) (b)

Fig. 5. Experimental result of the five-phase IPMSM starting up to 1.0 p.u. (a) multiscalar structure, (b) proposed multiscalar structure

In Fig. 6, the five-phase IPMSM drive was reversed from 1.0 p.u. to −1.0 p.u. The measured speed $(x_{11(1)})$, estimated speed $(\hat{x}_{11(1)})$, the error between the estimated speed and the measured speed for the first plane $(\tilde{x}_{11(1)})$, the generation of electromagnetic torque in the first plane and the second plane $(\hat{x}_{12(1)})$, are shown in Fig. 6a and 6b.

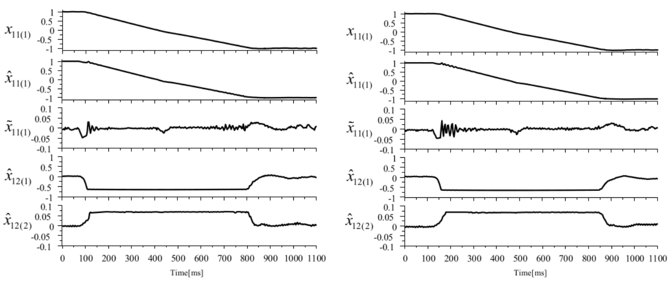

(a) (b)

Fig. 6. Experimental result of the five-phase IPMSM reversing from 1.0 p.u. to −1.0 p.u. (a) multiscalar control structure, (b) proposed control structure

In Figs. 5 and 6, the performance of the proposed control structure is compared with the classical control structure. It can be observed that behaviour of the proposed control system is almost the same as the classical control system. Moreover, the proposed control system is simple and also reduces the overall control efforts as a flux controlling controller is not required while in the classical control structure flux controlling controller is needed.

In Figs. 7 and 8, drive performance was examined for the case of load injection and removal at a low speed around 0.15 p.u., and at a medium speed around 0.5 p.u., respectively. In Figs. 7 and 8, important variables are shown such as the measured speed ($x_{11(1)}$), the estimated speed ($\hat{x}_{11(1)}$), the speed estimation error ($\tilde{x}_{11(1)}$), and the torque production in each plane ($\hat{x}_{12(1)}$, $\hat{x}_{12(2)}$). In Fig. 7a, the drive was running at a steady state around 0.15 p.u., without load. After 0.12 s, the load torque was changed to 0.45 p.u., with the torque production in the first plane ($\hat{x}_{12(1)}$) and the second plane ($\hat{x}_{12(1)}$) increasing up to 0.45 p.u. and 0.045 p.u., respectively. Similarly, in Fig. 7b the applied load was cut off as the load was removed, and the torque generation in each plane was reduced to 0.0 p.u. In Fig. 8a, the speed of the five-phase IPMSM was set at 0.5 p.u. and after 0.24 s the load torque was changed from 0.2 p.u. to 0.74 p.u. as shown. In Fig. 8b, the applied load was pulled out from 0.74 p.u.

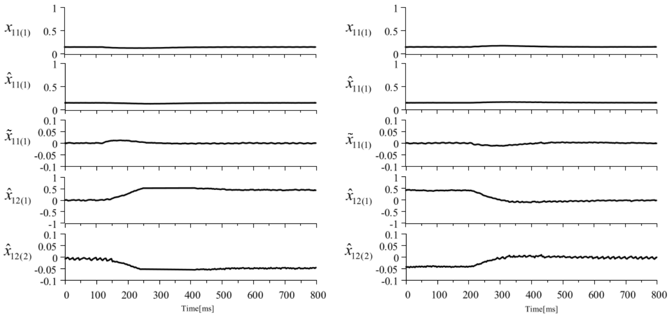

(a) (b)

Fig. 7. Experimental result of the loaded five-phase IPMSM at low speed around 0.15 p.u. (a) after 0.12 s load torque changed from 0.0 p.u. to 0.45 p.u., (b) after 0.2 s load torque fell from 0.45 p.u. to 0.0 p.u.

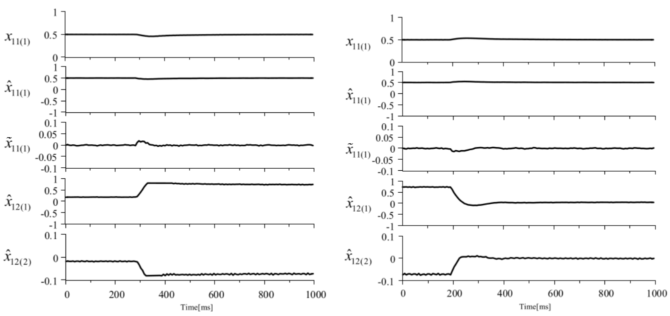

(a) (b)

Fig. 8. Experimental result of the loaded five-phase IPMSM (a) after 0.24 s the load torque changed from 0.2 p.u. to 0.74 p.u., (b) after 0.19 s the load torque fell 0.74 p.u. to 0.0 p.u.

to 0.0 p.u. after 0.19 s. During both tests, the calculated speed estimation error was almost close to zero.

The speed reversal of the five-phase IPMSM from 0.1 p.u. to −0.1 p.u is presented in Fig. 9a. Simultaneously, the speed of the second plane changed from −0.3 p.u. to 0.3 p.u., the flux level was kept at the desired level during low-speed reversal. The standstill test of the five-phase IPMSM is visible in Fig. 9b. The machine speed changed from 0.15 p.u. to 0.0 p.u after 0.4 s and again to 0.15 p.u. after 4.35 s. During this test, IPMSM did not remain at zero speed and returned to 0.15 p.u. without losing the synchronism.

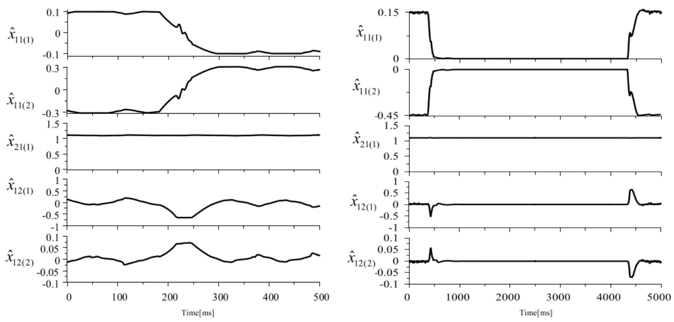

(a) (b)

Fig. 9. Experimental result of the unloaded five-phase IPMSM (a) machine reversed from 0.1 p.u. to −0.1 p.u., (b) standstill test, speed changed from 0.15 to 0.0 p.u.

In Fig. 10, the proposed control system was tested against the uncertainty of the machine parameters to check robustness. For this test, the angular speed of the first plane was set around 0.7 p.u., the speed of the second plane was 2.1 p.u., and the applied load torque was around 0.57 p.u. In Fig. 10a and 10b, the inductance of the $L_{q(1)}$ first plane and the $L_{q(2)}$ second plane varied for three different cases. $L_{q(1)}$ was equal to $0.5\,L_{qn(1)}$, and after 3.2 s $L_{q(1)} = L_{qn(1)}$, and again after 6.9 s $L_{q(1)}$ was equal to $1.5\,L_{qn(1)}$. Similarly, $L_{q(2)}$ was equal to $0.7\,L_{qn(2)}$, and after 2.1 s $L_{q(2)} = L_{qn(2)}$, and again after 6.2 s $L_{q(2)}$ was $1.7\,L_{qn(2)}$. From Fig. 10a, it can be observed that the system lost its stability when inductances of the first plane value changed

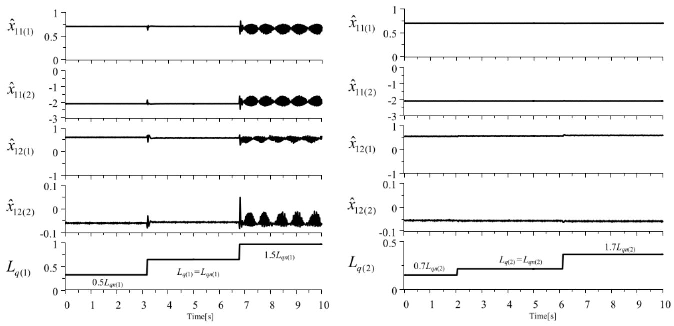

(a) (b)

Fig. 10. Experimental result of the five-phase IPMSM for different values of inductance, load torque = 0.57 p.u., machine speed was set at 0.7 p.u. (a) $L_{q(1)}$, (b) $L_{q(2)}$

$L_{q(1)} = 1.5\,L_{qn(1)}$. In Fig. 10b, the system remained stable for all the cases of inductance $L_{q(2)}$ variation in the second plane. In Table 4, similarities and differences between the classical multiscalar control scheme and the proposed multiscalar control scheme are given.

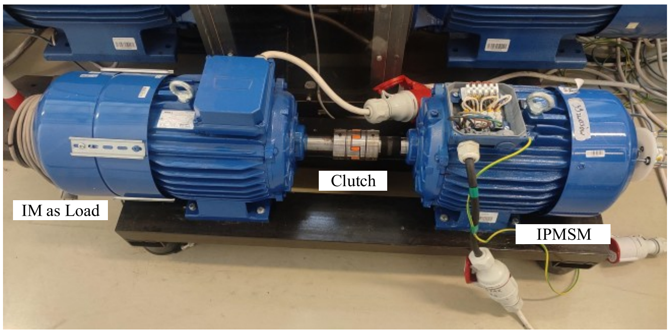

Fig. 11. Photograph of the experimental stand with the IPMSM clutched to IM

Table 4
Comparison of the control schemes for selected properties

Property	Classical multiscalar control	Proposed multiscalar control
Computation time (µs)	120	112
Decoupled control law	Yes	Yes
Number of controllers required	7	5
Complexity of gain tuning	High	Medium
Overshoot	< 5%	< 3%
Speed estimation error during the dynamic state	< 0.05 p.u.	< 0.04 p.u.

7. CONCLUSIONS

This article presented sensorless multiscalar control of the five-phase IPMSM. Based on the chosen multiscalar variables defined in Section 4, a multiscalar model is prepared. To linearize the multiscalar model, a new signal with nonlinear terms is provided as feedback. After the decoupling process, reference voltage signals are prepared for the PWM algorithm based on control signals. The proposed multiscalar control system of the five-phase IPMSM is compared with the classical multiscalar control scheme. The proposed control technique requires a smaller number of controllers to separately control the electromechanical subsystem and electromagnetic subsystem than the classical control scheme. The five-phase 5.5 kW IPMSM was used for experimental tests. All experimental results confirmed that the proposed control scheme provides excellent performance during different tests like drive start-up to nominal speed, speed reversal, load torque injection at low speed and medium speed, low-speed reversal and standstill test, and parameter uncertainty test. The speed and torque oscillations increased when $L_{q(1)}$ was 1.5 times the nominal value of inductance, which shows that overall stability was reduced, while the system remained stable for inductance $L_{q(2)}$ variation for all three cases.

REFERENCES

[1] S. Rubino, O. Dordevic, E. Armando, I.R. Bojoi, and E. Levi, "A Novel Matrix Transformation for Decoupled Control of Modular Multiphase PMSM Drives," *IEEE Trans. Power. Electron.*, vol. 36, no. 7, pp. 8088–8101, Jul. 2021, doi: 10.1109/TPEL.2020.3043083.

[2] E. Levi, F. Barrero, and M.J. Duran, "Multiphase machines and drives-revisited," *IEEE Trans. Ind. Electron.*, vol. 63, no. 1, pp. 429–432, 2016, doi: 10.1109/TIE.2015.2493510.

[3] B.M. Wilamowski and J. David Irwin, *Power Electronics and Motor Drives (The Industrial Electronics Handbook)*, Chapter 27, CRC Press, 2011.

[4] L. Parsa and H.A. Toliyat, "Five-phase permanent-magnet motor drives," *IEEE Trans. Ind. Appl.*, vol. 41, no. 1, pp. 30–37, Jan. 2005, doi: 10.1109/TIA.2004.841021.

[5] J. Li, B. Du, T. Zhao, Y. Cheng, and S. Cui, "Third-Harmonic Current Injection Control of Five-Phase Permanent-Magnet Synchronous Motor Based on Third-Harmonic Current Reference Online Identification," *IEEE Access*, vol. 11, pp. 41840–41847, 2023, doi: 10.1109/ACCESS.2023.3269282.

[6] G. Wang, M. Valla, and J. Solsona, "Position sensorless permanent magnet synchronous machine drives – A review," *IEEE Trans. Ind. Electron.*, vol. 67, no. 7, pp. 5830–5842, Jul. 2020, doi: 10.1109/TIE.2019.2955409.

[7] Xu D, Wang B, Zhang G, Wang G, and Yu Y, "A Review of Sensorless Control Methods for AC Motor Drives," *CES Trans. Electr. Mach. Syst.*, vol. 2, no. 1, pp. 104–115, 2018, doi: 10.23919/TEMS.2018.8326456.

[8] S.K. Sul and S. Kim, "Sensorless control of IPMSM: Past, present, and future," *IEEJ J. Ind. Appl.*, vol. 1, no. 1, pp. 15–23, 2012, doi: 10.1541/ieejjia.1.15.

[9] S. Sul, Y. Kwon, and Y. Lee, "Sensorless Control of IPMSM for Last 10 Years and Next 5 Years," *CES Trans. Electr. Mach. Syst.*, vol. 1, no. 2, pp. 91–99, 2017, doi: 10.23919/TEMS.2017.7961290.

[10] B. Tian, M. Molinas, and Q. An, "PWM Investigation of a Field-Oriented Controlled Five-Phase PMSM under Two-Phase Open Faults," *IEEE Trans. Energy Convers.*, vol. 36, no. 2, pp. 580–593, Jun. 2021, doi: 10.1109/TEC.2020.3029264.

[11] B. Tian, L. Sun, M. Molinas, and Q.T. An, "Repetitive Control Based Phase Voltage Modulation Amendment for FOC-Based Five-Phase PMSMs under Single-Phase Open Fault," *IEEE Trans. Ind. Electron.*, vol. 68, no. 3, pp. 1949–1960, Mar. 2021, doi: 10.1109/TIE.2020.2975502.

[12] W. Li, G. Feng, Z. Li, M.S. Toulabi, and N. Kar, "Extended Kalman Filter Based Inductance Estimation for Dual Three-Phase Permanent Magnet Synchronous Motors Under the Single Open-Phase Fault," *IEEE Trans. Energy Convers.*, vol. 37, no. 2, pp. 1134–1144, Jun. 2022, doi: 10.1109/TEC.2021.3129283.

[13] P. Song, W. Li, Z. Li, M.S. Toulabi, and N.C. Kar, "Noise and Vibration Prediction of a Six-Phase IPMSM in a Single Open-Phase Failure Under a Negative Sequence Current Compensated Fault Tolerant Control Mode," *IEEE Trans. Magn.*, vol. 58, no. 8, p. 8202806, Aug. 2022, doi: 10.1109/TMAG.2022.3146373.

[14] Z. Liu, Y. Li, and Z. Zheng, "A review of drive techniques for multiphase machines," *CES Trans. Electr. Mach. Syst.*, vol. 2, no. 2, pp. 243–251, Jun. 2018, doi: 10.30941/cestems.2018.00030.

[15] L. Zhang, X. Zhu, R. Cui, and S. Han, "A Generalized Open-Circuit Fault-Tolerant Control Strategy for FOC and DTC of Five-Phase Fault-Tolerant Permanent-Magnet Motor," *IEEE Trans. Ind. Electron.*, vol. 69, no. 8, pp. 7825–7836, Aug. 2022, doi: 10.1109/TIE.2021.3106012.

[16] F. Barrero and M.J. Duran, "Recent advances in the design, modeling, and control of multiphase machines – Part I," *IEEE Trans. Ind. Electron.*, vol. 63, no. 1, pp. 449–458, Jan. 2016, doi: 10.1109/TIE.2015.2447733.

[17] M.J. Duran and F. Barrero, "Recent advances in the design, modeling, and control of multiphase machines – Part II," *IEEE Trans. Ind. Electron.*, vol. 63, no. 1, pp. 459–468, Jan. 2016, doi: 10.1109/TIE.2015.2448211.

[18] R. Marino, P. Tomei, and C.M. Verrelli, *Advances in Industrial Control*. Springer London, 2010, doi: 10.1007/978-1-84996-284-1.

[19] M.S.R. Saeed, W. Song, B. Yu, and X. Feng, "Generalized Deadbeat Solution for Model Predictive Control of Five-Phase PMSM Drives," *IEEE Trans. Power Electron.*, vol. 38, no. 4, pp. 5178–5191, Apr. 2023, doi: 10.1109/TPEL.2022.3228074.

[20] Y. Luo, K. Yang, and Y. Zheng, "Luenberger Observer-Based Model Predictive Control for Six-Phase PMSM Motor With Localization Error Compensation," *IEEE Trans. Ind. Electron.*, vol. 70, no. 11, pp. 10800–10810, Nov. 2023, doi: 10.1109/TIE.2022.3229340.

[21] P.F.C. Goncalves, S.M.A. Cruz, and A.M.S. Mendes, "Disturbance Observer Based Predictive Current Control of Six-Phase Permanent Magnet Synchronous Machines for the Mitigation of Steady-State Errors and Current Harmonics," *IEEE Trans. Ind. Electron.*, vol. 69, no. 1, pp. 130–140, Jan. 2022, doi: 10.1109/TIE.2021.3053885.

[22] Y. Zafari, A.H. Mazinan, and S. Shoja-Majidabad, "Speed control of five-phase ipmsm through pi, smc and fitsmc approaches under normal and open phase faulty conditions," *Automatika*, vol. 58, no. 4, pp. 506–519, 2017, doi: 10.1080/00051144.2018.1478928.

[23] G. Liu, C. Geng, and Q. Chen, "Sensorless Control for Five-Phase IPMSM Drives by Injecting HF Square-Wave Voltage Signal into Third Harmonic Space," *IEEE Access*, vol. 8, pp. 69712–69721, 2020, doi: 10.1109/ACCESS.2020.2986347.

[24] I. Boldea, M.C. Paicu, and G.D. Andreescu, "Active flux concept for motion-sensorless unified AC drives," *IEEE Trans. Power Electron.*, vol. 23, no. 5, pp. 2612–2618, 2008, doi: 10.1109/TPEL.2008.2002394.

[25] I. Boldea, M.C. Paicu, G.D. Andreescu, and F. Blaabjerg, "'Active Flux' DTFC-SVM sensorless control of IPMSM," *IEEE Trans. Energy Convers.*, vol. 24, no. 2, pp. 314–322, 2009, doi: 10.1109/TEC.2009.2016137.

[26] R. Krishnan, *Permanent magnet synchronous and brushless DC motor drives*. CRC Press/Taylor & Francis, 2010.

[27] G. Wang, G. Zhang, and D. Xu, *Position Sensorless Control Techniques for Permanent Magnet Synchronous Machine Drives*. Springer Nature Singapore, 2020.

[28] D. Vyas, M. Morawiec, T. Ayana, L. Wogi, and J. Guziński, "Active flux based adaptive and non-adaptive observer for sensorless interior permanent magnet synchronous machine drive," *Arch. Electr. Eng.*, vol. 73, no. 3, pp. 799–815, 2024, doi: 10.24425/aee.2024.150896.

[29] D. Vyas, M. Morawiec, and D. Wachowiak, "Rotor flux and EEMF observer for interior permanent magnet synchronous machine," *Bull. Pol. Acad. Sci. Tech. Sci.*, vol. 72, no. 4, p. e150327, Jul. 2024, doi: 10.24425/bpasts.2024.150327.

[30] M. Morawiec, A. Lewicki, and C.I. Odeh, "Rotor-Flux Vector Based Observer of Interior Permanent Synchronous Machine," *IEEE Trans. Ind. Electron.*, vol. 71, no. 2, pp. 1399–1409, Feb. 2024, doi: 10.1109/TIE.2023.3250851.

[31] J. Guzinski, H. Abu-rub, and S. Patryk, *Variable Speed ac Drives with Inverter Output Filters*, 1st Ed, John Wiley & Sons, Ltd, 2015.